

Mechanics of Advanced Materials and Structures



ISSN: (Print) (Online) Journal homepage: https://www.tandfonline.com/loi/umcm20

Computational characterization of polymeric materials 3D-printed via fused filament fabrication

Narges Dialami, Ivan Rivet, Miguel Cervera & Michele Chiumenti

To cite this article: Narges Dialami, Ivan Rivet, Miguel Cervera & Michele Chiumenti (2022): Computational characterization of polymeric materials 3D-printed via fused filament fabrication, Mechanics of Advanced Materials and Structures, DOI: 10.1080/15376494.2022.2032496

To link to this article: https://doi.org/10.1080/15376494.2022.2032496

	Published online: 15 Feb 2022.
	Submit your article to this journal $oldsymbol{arOmega}$
Q ^L	View related articles 🗷
CrossMark	View Crossmark data 🗗



ORIGINAL ARTICLE



Computational characterization of polymeric materials 3D-printed via fused filament fabrication

Narges Dialami (D), Ivan Rivet (D), Miguel Cervera (D), and Michele Chiumenti (D)

Department of Civil and Environmental Engineering, International Center for Numerical Methods in Engineering (CIMNE), Technical University of Catalonia, Barcelona, Spain

ABSTRACT

This work develops a novel homogenization-based computational strategy for predicting the mechanical properties of fused filament fabricated parts by characterizing the component according to the different printing patterns used. The anisotropic constitutive material models obtained for each printing pattern allows the accurate prediction of the behavior of the entire component. The model is validated against experiments with the samples manufactured according to corresponding printing patterns. Various materials including Polycarbonate/Acrylonitrile Butadiene Styrene and ULTEM 9085 are tested. The good accuracy of the predictions obtained using present approach indicates that material characterization can be successfully performed in a fully numerical way.

ARTICLE HISTORY

Received 1 December 2021 Accepted 18 January 2022

KEYWORD

Additive manufacturing; material characterization; mechanical properties; computational homogenization; anisotropy

1. Introduction

3D-printing, also known as additive manufacturing (AM), is a process of layer by layer deposition of the material to build a 3D component. Due to its many advantages, such as material saving and facility to fabricate complex shapes, AM has attracted major interest of many industrial sectors.

Among the numerous AM techniques, fused filament fabrication (FFF) aims at printing 3D prototypes using polymeric materials [1, 2].

In FFF, material is extruded via a nozzle by melting the filaments and depositing them in a layer by layer manner on the printing platform enabling the fabrication of complex 3D structures (Figure 1).

FFF is studied and used by diverse groups of academics and industry professionals and application fields of this technology are continuously growing. To mention some of the most recent applications of FFF, Singh et al. [3] used recycled/virgin thermoplastics to print in house energy storage devices in shape of dry cell via FFF. Moreover, Vidakis et al. [4] used conductive polymer composites as feedstock materials in FFF with multifunctional performance to print low-priced customized biomedical components with complex features.

Similar to other AM techniques, the material properties of the printed FFF part can differ from that of the raw material [5]. Noticeably, the final behavior of the FFF components is anisotropic, in contrast to the isotropic behavior of the raw material. This behavior is the consequence of layer-to-layer and filament-to-filament adhesion as well as the printing patterns [6].

The process parameters such as the printing orientation, thickness and printing pattern selected prior to the printing procedure affect the quality and performance of the printed component [7]. Therefore, choosing appropriate process parameters and thus maximizing the performance of FFF parts is an important issue for the AM industries.

The printing patterns in a FFF structure is a combination of aligned filaments, crossed filaments (with 45° raster angle) and the selected pattern for the inner structure (lattice or infill; Figure 2). The aligned filaments dress most of the external surfaces while the crossed filaments dress only the top and bottom surfaces.

The inner structure pattern also affects the overall stiffness and behavior of the part. These inner structures are used in FFF components so as to reduce the weight and the amount of material, making FFF technique advantageous over other AM technologies in terms of raw material expenditure [8]. Considering that the amount of material can be greatly reduced in FFF, it is particularly important to ensure that the fabricated component provides the desired mechanical performance.

Prediction of the mechanical properties of the FFF components is a challenging task due to their inherent heterogeneity and anisotropy. Commonly, for the performance analysis of the FFF structures and verifying the effect of each printing parameters, the printed part is analyzed as a component made of a single material with given properties. Several research works have studied the effect of the printing orientation [9–14] and the effect of raster angle [15–21] on the final mechanical behavior of the component following this assumption.

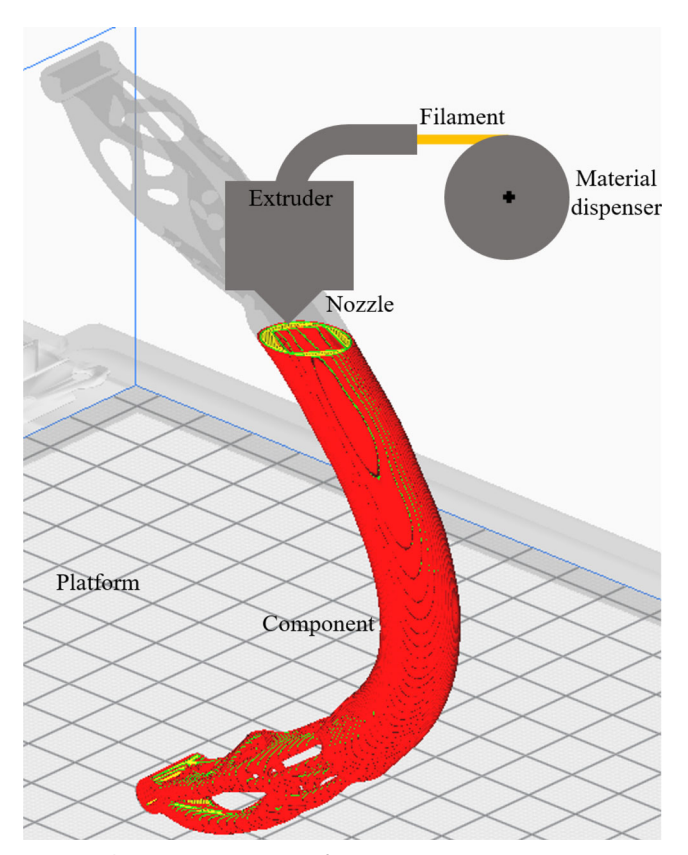


Figure 1. Schematic representation of FFF process.

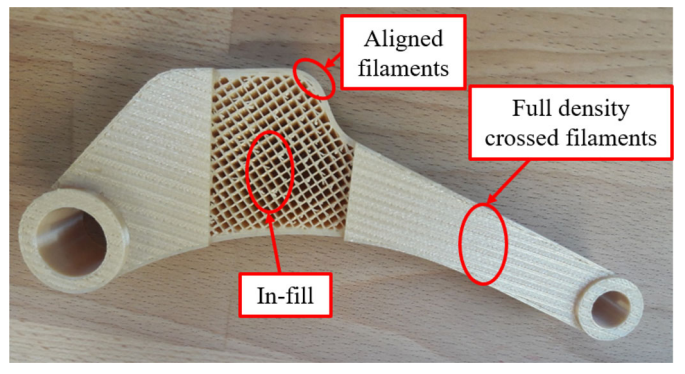


Figure 2. Printing patterns of a FFF component.

Casavola et al. [22] described the final orthotropic properties of the FFF parts of acrylonitrile butadiene styrene (ABS) and polylactic acid (PLA) using classical lamination theory (CLT). The orthotropic material behavior of the parts built in different orientations is assessed by experiment in [23, 24]. The experimental works reveal the effect of the built orientation and printing patterns on the final properties of the FFF parts [23-32]. From these works it is evident that the build orientation has a great role in the material behavior and characterization of the printed part. Therefore, the variation of the material behavior due to these two features has to be considered for the characterization of the part.

Rodriguez et al. [33, 34] presented a model for predicting the in-plane anisotropic elastic moduli of ABS materials. However, the model did not account for the elastic moduli of other material directions such as that of extruded fibers. The latter is essential to accurately evaluate the capability of the model as changes in polymer orientation affect its mechanical properties.

Nasirov et al. [35, 36] employed asymptotic homogenization to predict the mechanical properties of FFF infill structures by upscaling the properties from microscale to mesoscale and from mesoscale to macroscale.

In the latest work of Somireddy and Czekanski [37] the FFF parts of polymeric composite material were modeled using computational homogenization to estimate their final constitutive behavior. However, differentiation of the properties according to the printing patterns involved in a single component was not considered.

In the previous works of the authors [38, 39], each printing pattern used in a component represented a material with its corresponding properties (three printing patterns represented three materials). To feed the anisotropic material properties for the zones with aligned and crossed filaments, tensile tests were performed on the samples with the corresponding printing patterns. The in-fill was modeled using computational homogenization technique as a homogeneous material with an equivalent constitutive behavior.

In this article, we propose to take full advantage of the computational homogenization technique, not only for modeling the in-fill structure but also for the zones with aligned filaments as well as crossed filaments. The novelty of the model consists in the distinction among the material properties of the zones of a single printed component according to the printing patterns: aligned filaments, crossed filaments, and the inner structure. Anisotropic linear elastic constitutive models are considered for describing the mechanical behavior of each part of the component. Moreover, material properties of each part is identified computationally using a representative volume element (RVE). The materials studied in this work are general purpose acrylonitrile butadiene styrene (ABS GP), polycarbonate/acrylonitrile butadiene styrene (ABS-PC), PEI ULTEM 9085, and Polylactic Acid (PLA). The material properties obtained computationally are compared with the material properties of the samples tested experimentally in uniaxial tests.

The computational approach proposed in this work can be used as a design-for-manufacture (DFAM) strategy in order to create functional components.

2. Methodology

To characterize the material properties experimentally, nine parameters in the case of orthotropic material and five parameters in the case of a transversely isotropic one, it is necessary to perform tensile tests at 6 and 3 orientations, respectively (Figure 3). These tests have to be performed for each different printing pattern, multiplying the number of the tests. Moreover, several repetitions are needed for each test.

Contrariwise, the methodology developed in this work is fully based on the computational characterization of the materials printed by FFF.

A FFF component involves three printing patterns: (i) the zones with aligned filaments representing the contour of the component, (ii) the crossed filaments covering the top and

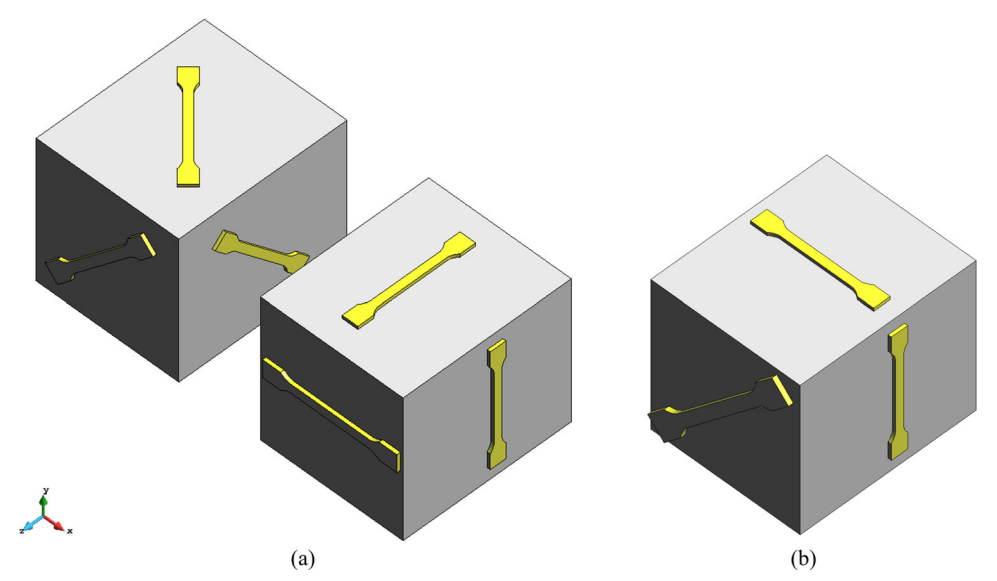


Figure 3. Printing orientations for material characterization (a) Orthotropic (b) Transversely isotropic.

bottom surfaces of the component, and (iii) the inner structure (in-fill or lattice) filling the inner part of the component with a certain density corresponding to raster to raster air gap.

The mechanical properties of the printed material are anisotropic and different from those of the isotropic raw material [5]. The degree of anisotropy depends on the printing pattern. It has a significant role on the material characterization.

In case of the top and bottom surfaces and the inner structure, the anisotropy is in the build direction. The stiffness is weaker than the inner-layer adhesion between printing layers. In case of the aligned filaments, the stiffness in the filament direction is greater than the intrafilament adhesion.

2.1. Constitutive model

To characterize the structural stiffness of FFF components, a linear elastic constitutive behavior is considered:

$$\sigma_m = C_m \epsilon_m \tag{1}$$

where σ_m and ϵ_m are the Cauchy stress and strain vectors, respectively. C_m is the constitutive (stiffness) matrix of the material. Reciprocally,

$$\epsilon_{m} = D_{m}\sigma_{m}$$
 (2)

where $D_m = C_m^{-1}$ is the compliance (flexibility) matrix. The compliance matrix of orthotropic materials is formed by 9 independent parameters: E_x , E_y , E_z , ν_{xy} , ν_{xz} , ν_{yz} , G_{xy} , G_{zx} , G_{yz} .

$$D_{m} = \begin{pmatrix} \frac{1}{E_{x}} & -\frac{\nu_{yx}}{E_{y}} & -\frac{\nu_{zx}}{E_{z}} & 0 & 0 & 0\\ -\frac{\nu_{xy}}{E_{x}} & \frac{1}{E_{y}} & -\frac{\nu_{zy}}{E_{z}} & 0 & 0 & 0\\ -\frac{\nu_{xz}}{E_{x}} & -\frac{\nu_{yz}}{E_{y}} & \frac{1}{E_{z}} & 0 & 0 & 0\\ 0 & 0 & 0 & \frac{1}{G_{yz}} & 0 & 0\\ 0 & 0 & 0 & 0 & \frac{1}{G_{zx}} & 0\\ 0 & 0 & 0 & 0 & 0 & \frac{1}{G_{xy}} \end{pmatrix}$$
(3)

where E_i is the Young's modulus along axis i, G_{ij} is the shear modulus in direction *j* on the plane whose normal is

in direction i, and ν_{ii} is the Poisson's ratio defining the relationship between the transversal deformation (direction j) and the axial elongation (when the loading is applied in direction i).

In FFF, as the components are printed in a layer by layer manner, the material properties can be considered as transversely isotropic. This means that the mechanical properties are symmetric in all directions of the transverse plane normal to an anisotropic principal axis along the deposition direction. If xy is the symmetry plane, the transversely isotropic material parameters are: $E = E_x = E_y$, E_z , ν_{xy} , ν_{zx} , $G = G_{zx} = G_{vz}$.

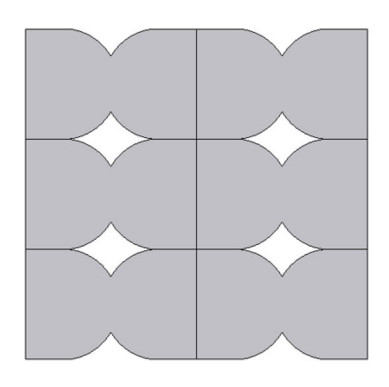
2.2. Computational homogenization

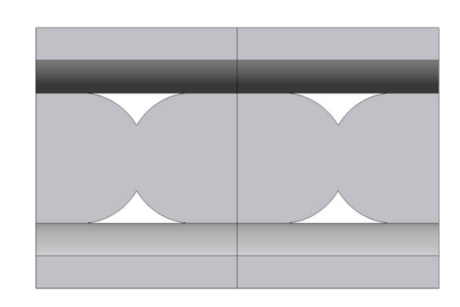
The stiffness matrices of the contour, the cover and the inner zone of the printed part can be calculated from the known properties of the raw material used for the printing. All the aforementioned zones of the single component represent a periodic architecture of the material (Figure 4). A small volume of the printed material as a Representative Volume Element (RVE) is considered for the computational homogenization (Figure 5). Shape, size, and distribution of the voids can vary depending on the filament dimension and the printing condition. Consequently, they affect the RVE dimension and shape.

In the homogenization technique, the RVE is considered as a macroscopically homogeneous orthotropic material. The homogenization technique involves macro and micro levels conforming to the FFF components and each separated zones, respectively [38, 39].

Following the steps described in Algorithm 1, to obtain the macroscopic homogenized constitutive matrix for each zone, macroscopic strains ϵ_m , are passed from the macro scale to the micro scale (down scaling) to solve the boundary value problem (BVP)

$$\int_{V_{DUE}} \nabla^{S} \tilde{\mathbf{v}}(\mathbf{x}) \sigma_{\mu}(\mathbf{x}) dV = 0 \tag{4}$$





(a) Aligned filaments of contour.



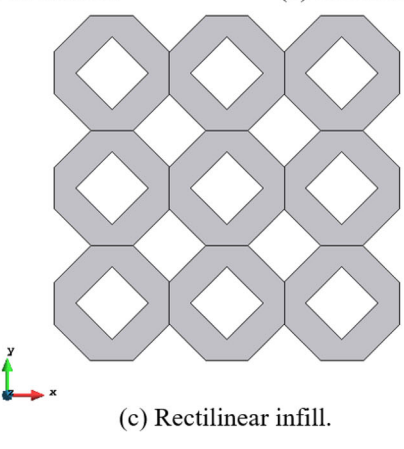


Figure 4. Printing patterns in a FFF component.

on the chosen RVE where the micro scale stress-strain relationship is

$$\sigma_{u}(x) = C_{u}(x)(\epsilon_{m}(X) + \nabla^{S}\tilde{u}(x))$$
 (5)

Functions \tilde{v} correspond to the Finite Element discretization of the RVE and \tilde{u} for the micro displacements' fluctuation. x stands for the coordinates at the microscale, and X at the macro scale. σ_{μ} is the microscopic stress field at each point x of the computational domain, C_{μ} the microscopic constitutive tensor and ϵ_{μ} microscopic strains.

Since the parts are made of a periodic material pattern, the RVEs are deformed periodically similar to the neighboring RVE. The Periodic Boundary Conditions (PBC) applied to the RVE models are

$$\tilde{\boldsymbol{u}}(\boldsymbol{x}^+) = \tilde{\boldsymbol{u}}(\boldsymbol{x}^-) \quad \forall \{\boldsymbol{x}^+ = \boldsymbol{x}^-\} \in \Gamma_{\text{RVE}}$$
 (6)

where x^+ and x^- are pairs of points corresponding to the opposite faces of the RVE boundary. Then after solving the RVE problem, the solution obtained at local level is *upscaled* to the macro level. The relationship between the local stresses σ_{μ} and global stresses σ_{m} is defined by

$$\sigma_{m}(X) = \frac{1}{V_{RVE}} \int_{V_{RVE}} \sigma_{\mu}(x) dV$$
 (7)

 C_m , the effective constitutive matrix of the anisotropic material is obtained

$$C_m = SE^{-1} \tag{8}$$

where E and S consist of 6 macroscopic strain and stress states given as $E = [\epsilon_m^{(1)} ... \epsilon_m^{(6)}]$ and $S = [\sigma_m^{(1)} ... \sigma_m^{(6)}]$, respectively.

Algorithm 1: First-order computational homogenization

Data: 6 representative macroscopic strain states: $\epsilon_m^{(1)}$, $\epsilon_m^{(2)}$, $\epsilon_m^{(3)}$, $\epsilon_m^{(4)}$, $\epsilon_m^{(5)}$ and $\epsilon_m^{(6)} \in \mathbb{R}^6$ (3 elongations and 3 distortions)

Result: the homogenized macro constitutive tensor $C_m \in \mathbb{R}^{6 \times 6}$ for k = 1 to 6 do

$$\begin{cases} \boldsymbol{\epsilon}_{m} \leftarrow \boldsymbol{\epsilon}_{m}^{(k)}; & /* \text{ Down-scaling }^{*/} \\ \text{ Solve the BVP } \int_{V_{RVE}} \nabla^{S} \tilde{\boldsymbol{\nu}} \boldsymbol{\sigma}_{\mu} dV = 0 \text{ applying the PBCs;} \\ \boldsymbol{\sigma}_{\mu} \leftarrow \boldsymbol{C}_{\mu} (\boldsymbol{\epsilon}_{m} + \nabla^{S} \tilde{\boldsymbol{u}}); & /* \text{ Up-scaling }^{*/} \\ \boldsymbol{\sigma}_{m} \leftarrow \frac{1}{V_{RVE}} \int_{V_{RVE}} \boldsymbol{\sigma}_{\mu} dV; & /* \text{ Up-scaling }^{*/} \\ \boldsymbol{\sigma}_{m}^{(k)} \leftarrow \boldsymbol{\sigma}_{m}; & \text{end} \end{cases}$$
 Form $\boldsymbol{E} \leftarrow [\boldsymbol{\epsilon}_{m}^{(1)} ... \boldsymbol{\epsilon}_{m}^{(6)}] \text{ and } \boldsymbol{S} \leftarrow [\boldsymbol{\sigma}_{m}^{(1)} ... \boldsymbol{\sigma}_{m}^{(6)}];$ $\boldsymbol{C}_{m} \leftarrow \boldsymbol{SE}^{-1};$

3. Computational characterization

This section presents the constitutive modeling of the parts with different printing patterns in a FFF component. The analysis is performed for four polymeric materials: ABS GP, ABS-PC, PLA, and PEI ULTEM 9085. First, the characterization of the material behavior using tensile tests is



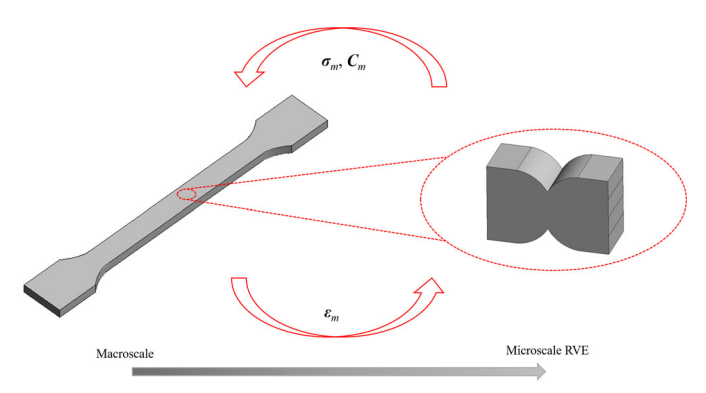


Figure 5. Homogenization framework.

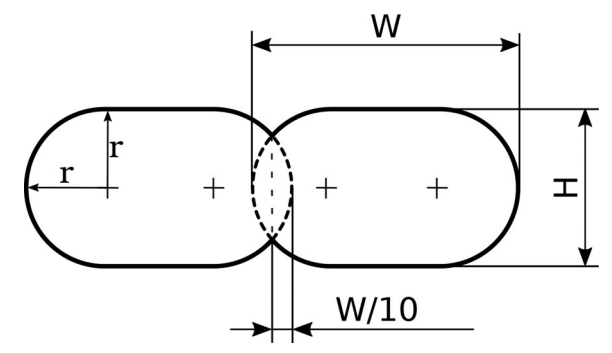


Figure 6. Simplified model of two adjacent filaments.

presented. Then, the stiffness matrix using the computational homogenization technique is determined. The computationally obtained material properties are validated with the results of tensile tests on samples made of the corresponding printing patterns.

In previous works of the authors [39], the computational homogenization technique for modeling the infill of FFF printed demonstrators has been validated. In this work, we focus on the contour and cover of the FFF components with aligned and crossed printing patterns, respectively. Moreover, for such printing patterns the experimental characterization is available.

3.1. Filaments material

Considering a 10% overlap between adjacent fibers according to the mesostructure [10] and due to their diffusion at the interface during solidification, the geometry of the cross section of two adjacent filaments is shown in Figure 6, where the height H and the width W depend on the printing parameters. Although the cross section of the fibers can be considered elliptical [40, 41], Garzon-Hernandez et al. [42] suggested that it was more realistic to characterize them as oblongs (a rectangle and two half-circles).

The heights and widths of the filaments cross section for ABS GP, ABS-PC, PLA, and PEI ULTEM 9085 are listed in Table 1.

The corresponding elastic parameters of the raw materials are given in Table 2. These isotropic properties are taken from Refs. [43–46]. However, these parameters can vary slightly depending on the manufacturer.

Table 1. Filaments cross section.

	PLA	ABS-GP	ABS-PC	PEI Ultem
Height (mm)	0.200	0.150	0.150	0.254
Width (mm)	0.400	0.400	0.450	0.508

Table 2. Raw material properties.

	PLA	ABS-GP	ABS-PC	PEI Ultem
Young's modulus (MPa)	3368	2100	2000	2600
Poisson's ratio	0.24	0.34	0.36	0.35

Table 3. Material properties characterized via tensile tests: Aligned filaments.

	E_x	E_{y}	E_z	G_{xy}	G_{xz}	G_{yz}			
	(GPa)	(GPa)	(GPa)	(GPa)	(GPa)	(GPa)	$ u_{xy}$	$\nu_{\it zx}$	ν_{zy}
PLA	2.50	2.50	3.05	1.01	0.94	0.94	0.24	0.24	0.24
ABS-GP	1.59	1.59	1.94	0.61	0.60	0.60	0.30	0.30	0.30
	±0.07	±0.07	± 0.05	±0.06	±0.05	±0.05	±0.06	±0.06	±0.06
ABS-PC	1.51	1.51	1.86	0.56	0.56	0.56	0.35	0.35	0.35
	±0.03	±0.03	±0.04	±0.01	±0.02	±0.02	±0.01	±0.01	±0.01
PEI Ultem	2.06	1.93	2.24	0.63	0.53	0.65	N/A	0.35	0.37
	±0.17	±0.07	±0.08	±0.03	±0.04	±0.05		±0.04	±0.04

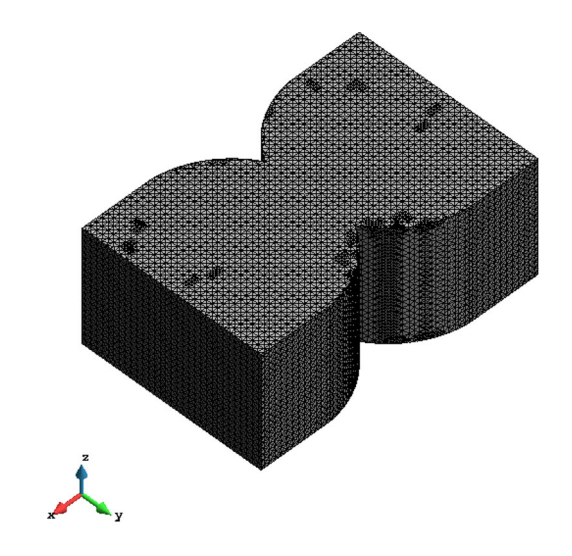


Figure 7. RVE corresponding to the aligned filaments of contour.

Table 4. Homogenized material properties: Aligned filaments.

	E_x	E_y	E_z	G_{xy}	G_{xz}	G_{yz}			
	(GPa)	(GPa)	(GPa)	(GPa)	(GPa)	(GPa)	ν_{xy}	$\nu_{\it zx}$	$\nu_{\it zy}$
PLA	2.59	2.11	3.09	0.98	1.10	1.00	0.25	0.24	0.24
ABS-GP	1.63	1.34	1.93	0.59	0.65	0.58	0.32	0.34	0.34
ABS-PC	1.56	1.28	1.83	0.56	0.61	0.55	0.34	0.36	0.36
PEI Ultem	2.02	1.67	2.39	0.72	0.80	0.71	0.33	0.35	0.35

3.2. Aligned filaments

For the experimental characterization of the contour material with the aligned filaments ASTM D638 dog-bone samples with the corresponding pattern have to be fabricated and tested. In previous works such samples have been tested and characterized [38, 39, 46]. Some of these tests focused on the transversely isotropic characterization of the material. For the characterization of the constitutive matrix, such tests include horizontal, vertical, and 45° printing orientations.

In the tensile tests, to obtain the Poisson's ratio, digital image correlation (DIC) is employed. DIC is a powerful

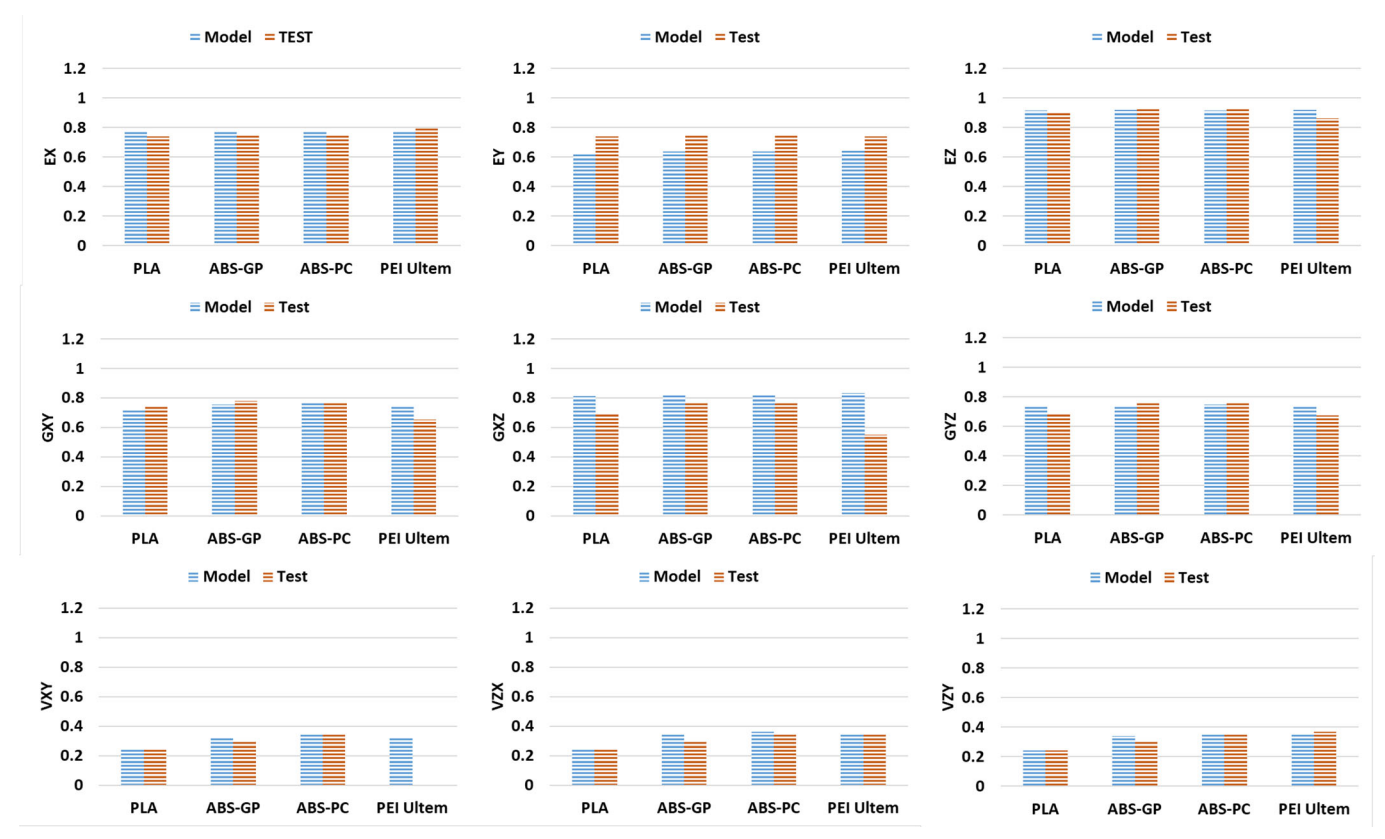


Figure 8. Normalized material properties. Aligned filaments.

experimental method for measuring full displacement and strain field. The fundamental idea of this technique lies in images comparison of a sample dressed with a speckle pattern before and after deformation, and by that to calculate the displacement and the strain fields as well as Poisson's ratio. This procedure is expensive. However, it is found in [39] that the effect of Poisson's ratio is minor on the final performance of the structure.

In case of contour material where the filaments are aligned, the transversely isotropic material properties obtained through the tensile tests are shown in Table 3.

The computational homogenization analysis is performed using the open source Kratos multiphysics finite element code [47]. As explained in Algorithm 1, the RVE is subjected to six diverse strains, applied separately by PBC in Eq. (6). This implies that six distinctive uniaxial and shear load cases are arranged for six strains to obtain the unknowns of the constitutive matrix. The RVE depends on the process parameters and the printing pattern. RVEs are oriented guaranteeing that their mesostructure is accurately oriented with reference to the load direction. After performing the finite element simulation for the homogenization of the material, the unknowns of the orthotropic matrix are obtained.

The RVE of the aligned filaments is taken from the mesostructure [10] and presented in Figure 7. The mesostructure is parametrically modeled for the computational homogenization analysis in order to obtain the macromechanical properties. The RVE is discretized by approximately 280,000 tetrahedral elements.

The orthotropic material properties obtained through the homogenization are presented in Table 4. A comparison between the tests and computational results is plotted in Figure 8. The normalized properties are nondimensional properties referring to the ratio of the obtained parameters, experimentally or computationally, with respect to the raw material properties. The agreement between the numerical and experimental material parameters is truly remarkable.

There is a slight difference between the E_y values obtained via homogenization and tensile test in case of ABS-GP and ABS-PC. This difference can be the result of the experimental set up. The tests were set so that transversely isotropic behavior of the material, rather than fully orthotropic, is characterized. Also, the underestimation of E_y may also be correlated to the assumption that the filaments are perfectly distributed along the cross-section, producing perfect diamond voids [48]. These voids can actually be triangle-shaped [42], a fact that implies a lower void fraction and thus an increase in the value of E_y .

Differences in the fabrication process cause the dispersion in the resulting parameters. For instance, printing at room temperature can cause great variability from one batch of specimens to another. The use of thermal chamber reduces the temperature gradient between the deposited filaments, strengthening the unions between layers, enhancing the mechanical behavior and reducing the degree of orthotropy.

To illustrate the computational procedure, Figure 9 presents the stress distribution (in terms of the von Mises stress) in RVEs subjected to 6 different strains using PBC to

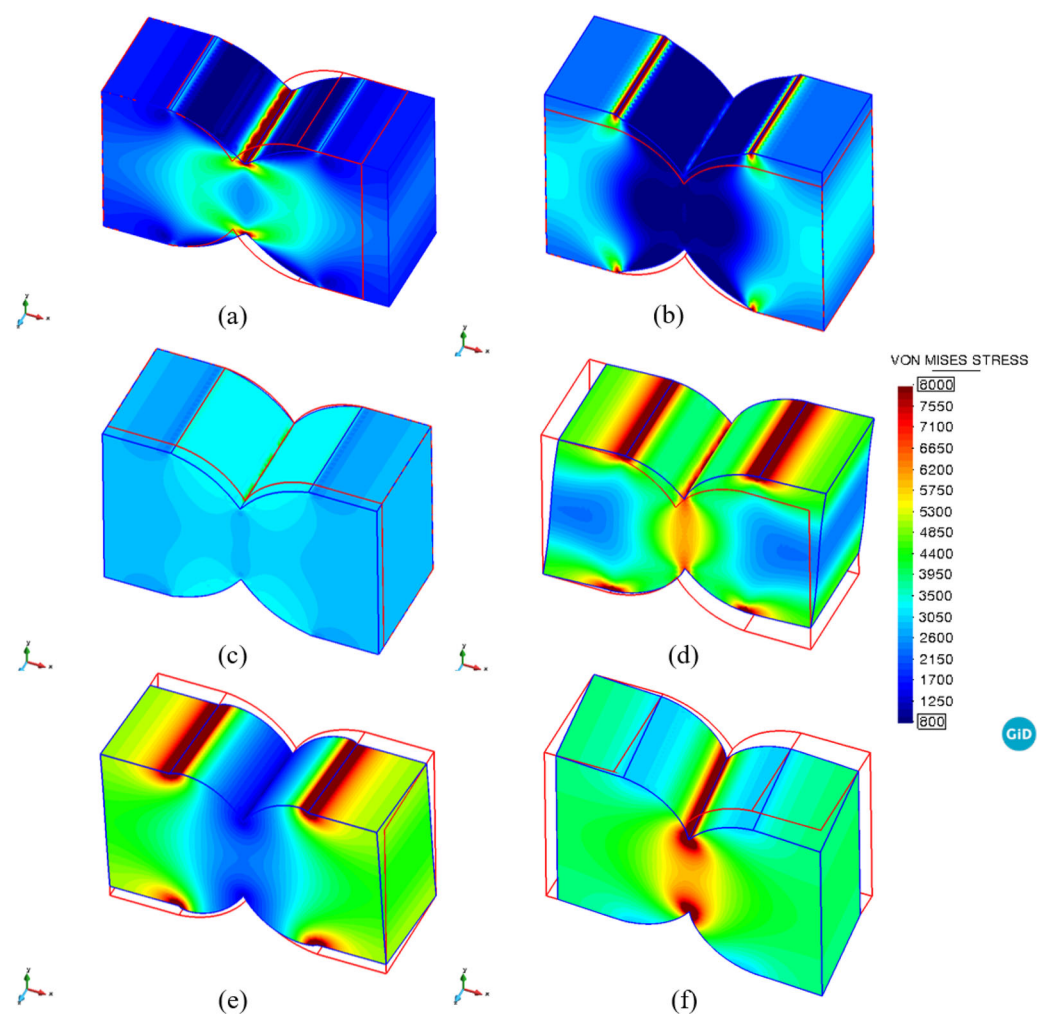


Figure 9. Stress distribution in RVE of contour subjected to six different strains. (a) ϵ_{xxy} (b) ϵ_{yyy} (c) ϵ_{zzy} (d) ϵ_{yzy} (e) ϵ_{yzz} (f) ϵ_{xz} .

Table 5. Material properties characterized via tensile tests: Crossed filaments.

Table 37 Material properties characterized the tensile tests crossed manierits.									
	<i>E_x</i> (GPa)	E_y (GPa)	E_z (GPa)	G _{xy} (GPa)	G_{xz} (GPa)	<i>G_{yz}</i> (GPa)	ν_{xy}	ν_{zx}	ν_{zy}
PLA	2.42	2.42	1.42	0.98	1.21	1.21	0.24	0.24	0.24
ABS-GP	1.54	1.54	0.90	0.58	0.45	0.45	0.33	0.33	0.33
	±0.07	±0.07	±0.31	±0.06	±0.11	±0.11	±0.07	±0.07	±0.07
ABS-PC	1.51	1.51	1.53	0.56	0.23	0.23	0.35	0.35	0.35
	±0.5	±0.5	±0.09	±0.2	±0.02	±0.02	±0.01	±0.01	±0.01
PEI Ultem	2.13	2.15	2.09	0.75	0.74	0.63	N/A	0.39	0.34
	±0.06	±0.19	±0.11	±0.09	±0.09	±0.08		±0.00	±0.03

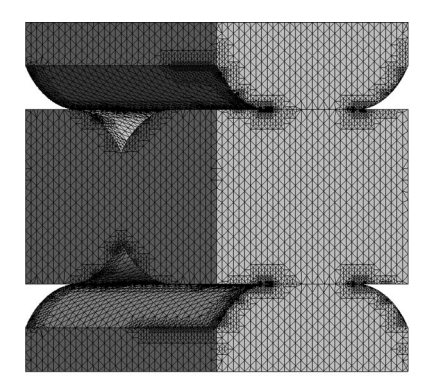




Figure 10. RVE corresponding to crossed filaments of cover.

Table 6. Homogenized material properties: Crossed filaments.

	E_x	E_y	E_z	G_{xy}	G_{xz}	G_{yz}			
	(GPa)	(GPa)	(GPa)	(GPa)	(GPa)	(GPa)	ν_{xy}	$\nu_{\it zx}$	$\nu_{\it zy}$
PLA	2.87	2.87	1.42	1.01	0.74	0.74	0.24	0.22	0.24
ABS-GP	1.75	1.75	0.88	0.68	0.68	0.68	0.33	0.33	0.33
ABS-PC	1.79	1.79	1.47	0.65	0.60	0.60	0.34	0.35	0.35
PEI Ultem	2.33	2.33	1.91	0.85	0.78	0.78	0.33	0.34	0.34

determine the anisotropic material parameters. The original undeformed boundary of the geometry is shown in red.

Considering the contour RVE (Figure 9), in all the cases the maximum stress appears at the conjunction between the filaments, the weakest part of the mesostructure. Debonding between the filaments can occur in the first loading case (Figure 9(a)) where ϵ_{xx} is applied. Therefore, these types of loading can be a cause of failure in such structures.

3.3. Crossed filaments

In case of cover material where the filaments are crossed, the experimentally characterized transversely isotropic material properties of the cover through the tensile tests are shown in Table 5.

The RVE of the crossed filaments taken from the mesostructure [10] is presented in Figure 10. The RVE is

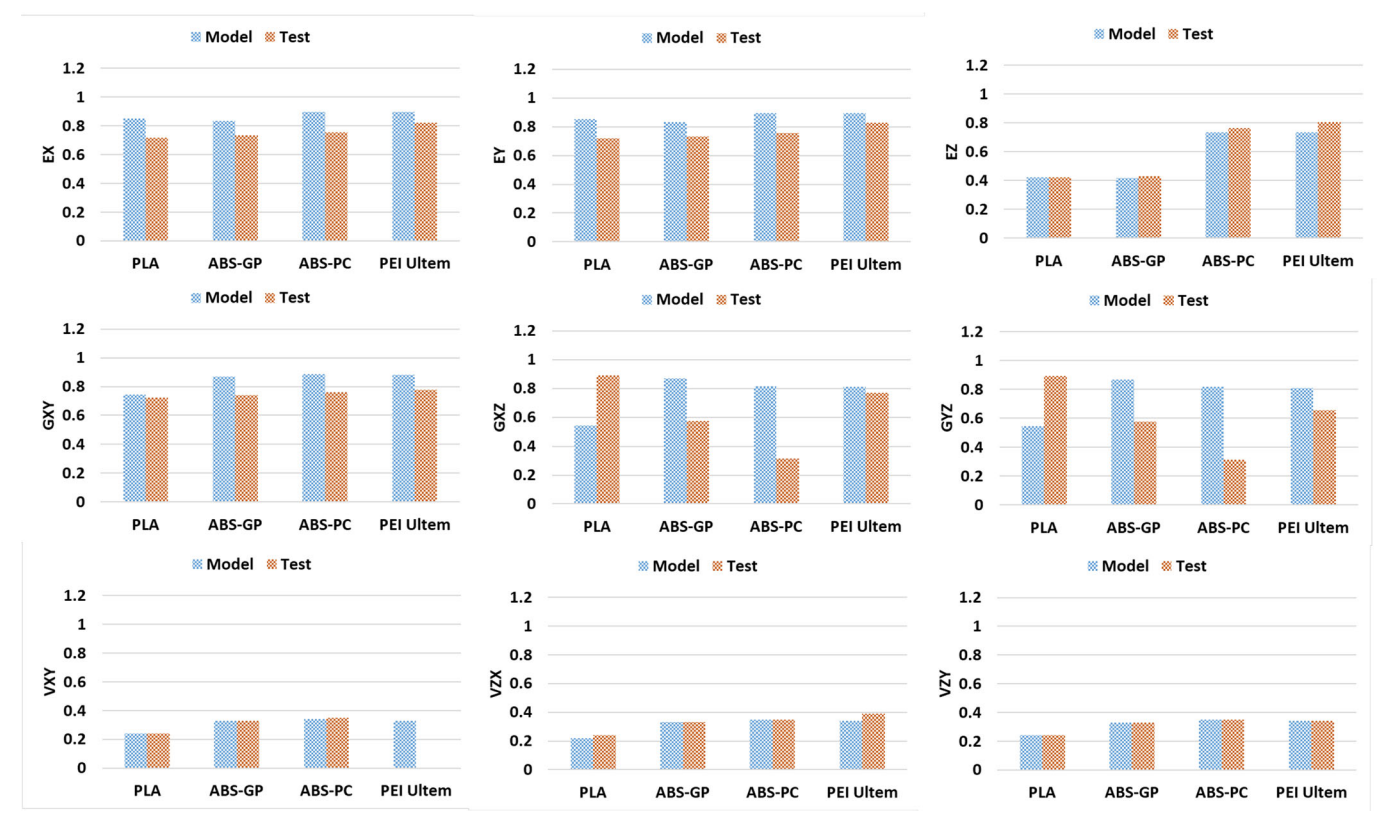


Figure 11. Normalized material properties. Crossed filaments.

discretized by approximately 310,000 tetrahedral elements. The anisotropic material properties obtained through the homogenization technique are presented in Table 6. A comparison between the experiments and the model results is plotted in Figure 11.

The agreement between the numerical and experimental material parameters is remarkable for most of them. Regarding the differences obtained for the shear moduli affecting the vertical planes, several remarks are in order:

- a. The layer thickness in the experiment due to the layer-to-layer filament overlap is lower than the numerical model where the preprinted filaments dimensions are considered. An increase in layer thickness decreases the stiffness of polymeric products as shown in [48];
- b. Since in the present computational model it is assumed that the bonding between adjacent filaments and between adjacent layers is perfect, it follows that most of the predicted stiffness are higher than the measured ones. The only property that does not follow this trend is E_z , which is greater in the experiments than in the model results. In order to be able to capture this, an inter-layer adhesion model has to be considered. The obtained results demonstrate that the intra-layer and the inter-layer adhesion play a significant role in the behavior of the FFF samples;
- c. Differences in the fabrication process cause the dispersion in the resulting material parameters. The effect of thermal chamber and reducing the degree of orthotropy is visible in the ABS-PC and Ultem crossed samples. Moreover, the ABS-PC properties depend on the ratio

of PC and ABS in the blend. ABS-PC features a remarkable impact resistance at low temperatures that is better than impact resistance of ABS or PC, separately. Therefore, ABS-PC presents a higher stiffness in the printing direction than ABS-GP. Similarly, Ultem exhibits an excellent strength-to weight ratio and impact strength with large heat resistance, as well as flame-retardant capacity.

These items affect each distinct material quite differently. It can be seen that in case of PEI Ultem, the agreement between the experimental and numerical material parameters is remarkable also for the shear moduli of the vertical planes.

To illustrate the computational procedure, Figure 12 presents the stress distribution (in terms of the von Mises stress) in RVEs subjected to six different strains using PBC in order to determine the anisotropic material parameters. The original undeformed boundary of the geometry is shown in red.

Considering the cover RVE (Figure 12), in all the cases the maximum stress appears at the conjunction between the filaments. The second loading case (Figure 12(b)) where ϵ_{yy} is applied has more tendency to cause the failure of the structure at the conjunction between the filaments than the other loading cases.

3.4. Discussion

Based on the experimental and computational results obtained, Young's modulus, shear modulus and Poisson's

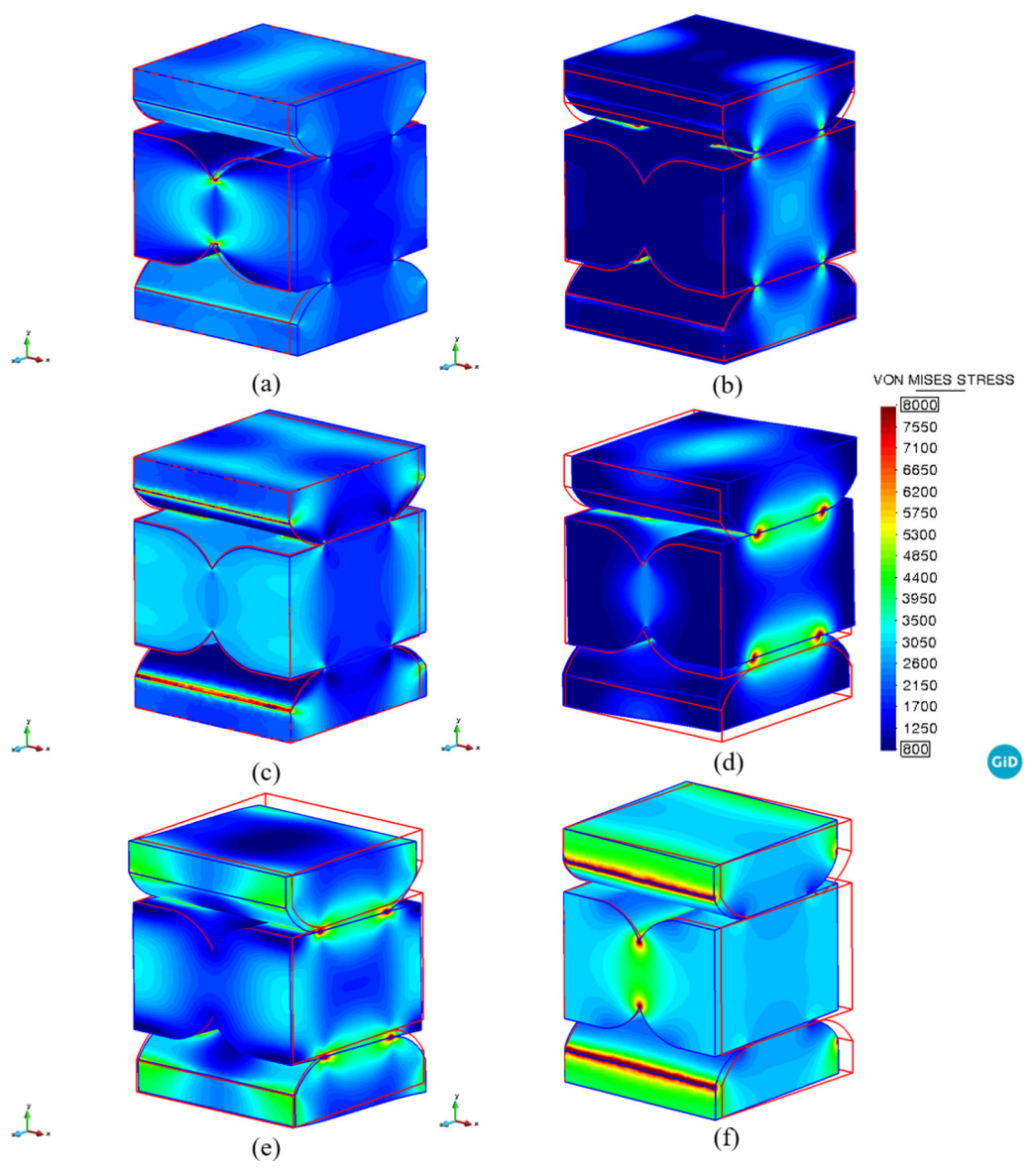


Figure 12. Stress distribution in RVE of cover subjected to 6 different strains. (a) ϵ_{xx_1} (b) ϵ_{yy_1} (c) ϵ_{zz_1} (d) ϵ_{xy_1} (e) ϵ_{yz_1} (f) ϵ_{xz_2}

ratio depend on the printing orientation. In case of aligned filaments E_z , Young's modulus on the filament direction, is higher than Young's moduli on the other two directions, being E_z the stiffest one. However, this behavior is quite the opposite in case of crossed filaments. Due to the elliptical shape of the filaments, the contour material behaves orthotropically, while the cover material behaves as transversely isotropic due to the symmetric pattern of the xy plane. The obtained numerical results are accurate and close enough to the experimental ones.

The layer thickness and the overlap among the adjacent strands are the driving parameters causing the differences with the experimental tests. In the computational model, the bonding between the adjacent strands is considered perfect while this is not the case in the real printed specimen. Also, the mesostructure depicted in this work is not the exact replication of the specimen's mesostructure used in the experiments causing the differences between the experimental and numerical studies.

4. Summary and conclusion

In this work, the mechanical properties of parts manufactured via FFF are predicted using a computational homogenization technique. As the material behavior varies with the variation of the printing patterns (aligned and crossed) present in a single component, differing from that of the raw material, each one of them is characterized separately. The numerical simulations results show good agreement compared with experimental tensile tests. Although isotropic materials are used for the printing, the mechanical behavior of each part is anisotropic due to the printing pattern and process parameters.

The numerical approach developed in this work has the capability of predicting the elastic properties of subcomponents of 3D-printed structures with different printing patterns. This methodology results in a significant reduction of the number of experimental tests necessary for the characterization of the 3D printed parts.

The results are obtained for standard printing conditions with perfect bonding between the adjacent strands, but they can be extrapolated to any process parameters by modifying the geometry of the RVE appropriately. Thus, the proposed methodology can be applied to a wide range of cases.

Depending on the filament dimensions and the printing conditions, the size and shape of the voids between the layers and filaments may vary, affecting the characterized material properties.

A decrease in the layer thickness due to the overlap of adjacent filaments of different layers increases the stiffness of polymeric products.

The FE microstructural simulation on a RVE allows the identification of the localized stress at the interfaces between the adjacent filaments and printing layers, and thus, the prediction of failure modes in FFF parts. It is found that debonding between the filaments and the failure of the FFF structure may be caused by the loading cases where ϵ_{xx} (direction perpendicular to the filament and printing axes) and ϵ_{yy} (printing direction) are applied in case of aligned and crossed filaments, respectively.

Acknowledgment

Narges Dialami is a Serra Húnter fellow.

Funding

This work has been supported by the European Union's Horizon 2020 Research and Innovation Programme (H2020-DT-2019-1 No. 872570) under the KYKLOS 4.0 Project (An Advanced Circular and Agile Manufacturing Ecosystem based on rapid reconfigurable manufacturing process and individualized consumer preferences) and by the Ministry of Science, Innovation and Universities (MCIU) via: the PriMuS project (Printing pattern based and MultiScale enhanced performance analysis of advanced Additive Manufacturing components, ref. num. PID2020-115575RB-I00). The financial support from the Spanish Ministry of Economy and Competitiveness, through the Severo Ochoa Programme for Centers of Excellence in R&D (CEX2018-000797-S), is gratefully acknowledged as well as from CONCYTEC R+D (Project Reference: 163-2017-FONDECYT, in association with Pontifical Catholic University of Perú and CIMNE) -" Optimización del uso de polímeros sintéticos en procesos de manufactura aditiva mediante modelos de simulación computacional y técnicas de caracterización de materiales. Caso de estudio: aplicaciones médicas - prótesis de mano."

ORCID

Narges Dialami (D) http://orcid.org/0000-0003-3115-7249
Ivan Rivet (D) http://orcid.org/0000-0002-8710-2733
Miguel Cervera (D) http://orcid.org/0000-0003-3437-6703
Michele Chiumenti (D) http://orcid.org/0000-0002-6286-7393

References

- [1] S.C. Ligon, R. Liska, J. Stampfl, M. Gurr, and R. Mulhaupt, Polymers for 3D printing and customized additive manufacturing, Chem. Rev., vol. 117, no. 15, pp. 10212–10290, 2017. DOI: 10.1021/acs.chemrev.7b00074.
- [2] B. Brenken, E. Barocio, A. Favaloro, V. Kunc, and R.B. Pipes, Fused filament fabrication of fiber-reinforced polymers: A review, Addit. Manuf., vol. 21, pp. 1–16, 2018. DOI: 10.1016/j. addma.2018.01.002.

- [3] R. Singh, H. Singh, I. Farina, F. Colangelo, and F. Fraternali, On the additive manufacturing of an energy storage device from recycled material, Compos. B Eng., vol. 156, pp. 259–265, 2019. DOI: 10.1016/j.compositesb.2018.08.080.
- [4] Nectarios Vidakis, Markos Petousis, Emmanuel Velidakis, Nikolaos Mountakis, Peder Erik Fischer-Griffiths, Sotirios Grammatikos, and Lazaros Tzounis, Fused filament fabrication three-dimensional printing Multi-functional of polylactic acid/ carbon black nanocomposites, C., vol. 7, no. 3, pp. 52, 2021. DOI: 10.3390/c7030052.
- [5] J. Kotlinski, Mechanical properties of commercial rapid prototyping materials, Rapid Prototyp. J., vol. 20, no. 6, pp. 499–510, 2014. DOI: 10.1108/RPJ-06-2012-0052.
- [6] A. Khudiakova, F. Arbeiter, M. Spoerk, M. Wolfahrt, D. Godec, and G. Pinter, Inter-layer bonding characterisation between materials with different degrees of stiffness processed by fused filament fabrication, Addit. Manuf., vol. 28, pp. 184–193, 2019. DOI: 10.1016/j.addma.2019.05.006.
- [7] H. Li, T. Wang, J. Sun, and Z. Yu, The effect of process parameters in fused deposition modelling on bonding degree and mechanical properties, Rapid Prototyp. J., vol. 24, no. 1, pp. 80–92, 2018. DOI: 10.1108/RPJ-06-2016-0090.
- [8] B.A. Aloyaydi, S. Sivasankaran, and H.R. Ammar, Influence of infill density on microstructure and flexural behavior of 3D printed PLA thermoplastic parts processed by fusion deposition modeling, Aims Mater. Sci., vol. 6, no. 6, pp. 1033–1048, 2019. DOI: 10.3934/matersci.2019.6.1033.
- [9] S.H. Ahn, M. Montero, D. Odell, S. Roundy, and P.K. Wright, Anisotropic material properties of fused deposition modeling ABS, Rapid Prototyp. J., vol. 8, no. 4, pp. 248–257, 2002. DOI: 10.1108/13552540210441166.
- [10] M. Somireddy, A. Czekanski, and C.V. Singh, Development of constitutive material model of 3D printed structure via FDM, Mater. Today Commun., vol. 15, pp. 143–152, 2018. DOI: 10. 1016/j.mtcomm.2018.03.004.
- [11] R. Zou et al., sotropic and anisotropic elasticity and yielding of 3D printed material, Compos. B Eng., vol. 99, pp. 506–513, 2016. DOI: 10.1016/j.compositesb.2016.06.009.
- [12] J.R.C. Dizon, A.H. Espera Jr., Q. Chen, and R.C. Advincula, Mechanical characterization of 3D-printed polymers, Addit. Manuf., vol. 20, pp. 44–67, 2018. DOI: 10.1016/j.addma.2017.12.002.
- [13] D. Popescu, A. Zapciu, C. Amza, F. Baciu, and R. Marinescu, FDM process parameters influence over the mechanical properties of polymer specimens: A review, Polym. Test., vol. 69, pp. 157–166, 2018. DOI: 10.1016/j.polymertesting.2018.05.020.
- [14] C. Gabor, M.A. Pop, D. Magli, T. Bedo, S.I. Munteanu, and D. Munteanu, The optimization of the production procedure in relation to the mechanical properties of additively manufactured parts, Mater. Today: Proc., vol. 19, pp. 1008–1013, 2019. DOI: 10.1016/j.matpr.2019.08.014.
- [15] C. Ziemian, M. Sharma, and S. Ziemian, Anisotropic mechanical properties of ABS parts fabricated by fused deposition modelling, Mech. Eng., vol. 23, pp. 2397, 2012.
- [16] J.C. Riddick, M.A. Haile, R. Von Wahlde, D.P. Cole, O. Bamiduro, and T.E. Johnson, Fractographic analysis of tensile failure of acrylonitrilebutadiene-styrene fabricated by fused deposition modeling, Addit. Manuf., vol. 11, pp. 49–59, 2016. DOI: 10.1016/j.addma.2016.03.007.
- [17] S. Ziemian, M. Okwara, and C.W. Ziemian, Tensile and fatigue behavior of layered acrylonitrile butadiene styrene, Rapid Prototyp. J., vol. 21, no. 3, pp. 270–278, 2015. DOI: 10.1108/ RPI-09-2013-0086.
- [18] B. Huang and S. Singamneni, Raster angle mechanics in fused deposition modelling, J. Compos. Mater., vol. 49, no. 3, pp. 363–383, 2015. DOI: 10.1177/0021998313519153.
- [19] D. Jiang and D.E. Smith, Anisotropic mechanical properties of oriented carbon fiber filled polymer composites produced with fused filament fabrication, Addit. Manuf., vol. 18, pp. 84–94, 2017. DOI: 10.1016/j.addma.2017.08.006.

- J. Torres, J. Cotelo, J. Karl, and A.P. Gordon, Mechanical property optimization of FDM PLA in shear with multiple objectives, JOM., vol. 67, no. 5, pp. 1183-1193, 2015. DOI: 10.1007/ s11837-015-1367-y.
- [21] B. Rankouhi, S. Javadpour, F. Delfanian, and T. Letcher, Failure analysis and mechanical characterization of 3D printed ABS with respect to layer thickness and orientation, J. Fail. Anal. Preven., vol. 16, no. 3, pp. 467-481, 2016. DOI: 10.1007/ s11668-016-0113-2.
- C. Casavola, A. Cazzato, V. Moramarco, and C. Pappalettere, Orthotropic mechanical properties of fused deposition modelling parts described by classical laminate theory, Mater. Des., vol. 90, pp. 453-458, 2016. DOI: 10.1016/j.matdes.2015.11.009.
- [23] A. Bellini and S. Güçeri, Mechanical characterization of parts fabricated using fused deposition modeling, Rapid Prototyp. J., vol. 9, no. 4, pp. 252-264, 2003. DOI: 10.1108/13552540310489631.
- M. Domingo-Espin, J.M. Puigoriol-Forcada, A.A. Garcia-Granada, J. Llumà, S. Borros, and G. Reyes, Mechanical property characterization and simulation of fused deposition modeling Polycarbonate parts, Mater. Des., vol. 83, pp. 670-677, 2015. DOI: 10.1016/j. matdes.2015.06.074.
- [25] K. Thrimurthulu, P.M. Pandey, and N.V. Reddy, Optimum part deposition orientation in fused deposition modeling, Int. J. Mach. Tools Manuf., vol. 44, no. 6, pp. 585-594, 2004. DOI: 10.1016/j.ijmachtools.2003.12.004.
- [26] P. Delfs, M. Tows, and H.J. Schmid, Optimized build orientation of additive manufactured parts for improved surface quality and build time, Addit. Manuf., vol. 12, pp. 314-320, 2016. DOI: 10.1016/j.addma.2016.06.003.
- T.D. McLouth, J.V. Severino, P.M. Adams, D.N. Patel, and R.J. Zaldivar, The impact of print orientation and raster pattern on fracture toughness in additively manufactured ABS, Addit. Manuf., vol. 18, pp. 103-109, 2017. DOI: 10.1016/j.addma.2017.09.003.
- [28] J. MartÝnez, J. DíEguez, J. Ares, A. Pereira, and J. Pérez, Modelization and structural analysis of FDM parts, AIP Conf. Proc., Vol. 1431, pp. 842-848, 2012.
- [29] I. Durgun and R. Ertan, Experimental investigation of FDM process for improvement of mechanical properties and production cost, Rapid Prototyp. J., vol. 20, no. 3, pp. 228-235, 2014. DOI: 10.1108/RPJ-10-2012-0091.
- C.W. Ziemian, R.D. Ziemian, and K.V. Haile, Characterization of stiffness degradation caused by fatigue damage of additive manufactured parts, Mater. Des., vol. 109, pp. 209-218, 2016. DOI: 10.1016/j.matdes.2016.07.080.
- [31] Jason Cantrell, Sean Rohde, David Damiani, Rishi Gurnani, Luke DiSandro, Josh Anton, Andie Young, Alex Jerez, Douglas Steinbach, Calvin Kroese, and Peter Ifju, Experimental characterization of the mechanical properties of 3D-printed ABS and polycarbonate parts, Rapid Prototyp. J., vol. 23, no. 4, pp. 811-824, 2017. DOI: 10.1108/RPJ-03-2016-0042.
- R. Zaldivar, D. Witkin, T. McLouth, D. Patel, K. Schmitt, and J. Nokes, Influence of processing and orientation print effects on the mechanical and thermal behavior of 3D-Printed ULTEM® 9085 Material, Addit. Manuf., vol. 13, pp. 71-80, 2017. DOI: 10.1016/j.addma.2016.11.007.
- [33] J., Rodriguez, Modeling the Mechanical Behavior of Fused Acrylonitrile-Butadiene-Styrene Components. Ph.D. thesis. University of Notre Dame, 1999.
- [34] J.F. Rodriguez, J.P. Thomas, and J.E. Renaud, Mechanical behavior of acrylonitrile butadiene styrene fused deposition

- materials modeling, Rapid Prototyp. J., vol. 9, no. 4, pp. 219-230, 2003. DOI: 10.1108/13552540310489604.
- A. Nasirov and I. Fidan, Prediction of mechanical properties of fused filament fabricated structures via asymptotic homogenization, Mech. Mater., vol. 145, pp. 103372, 2020. DOI: 10.1016/j.mechmat. 2020.103372.
- A. Nasirov, A. Gupta, S. Hasanov, and I. Fidan, Three-scale [36] asymptotic homogenization of short fiber reinforced additively manufactured polymer composites, Compos. B Eng., vol. 202, pp. 108269, 2020. DOI: 10.1016/j.compositesb.2020.108269.
- [37] M. Somireddy and A. Czekanski, Computational modeling of constitutive behaviour of 3D printed composite structures, J. Mater. Res. Technol., vol. 11, pp. 1710-1718, 2021. DOI: 10. 1016/j.jmrt.2021.02.030.
- [38] N. Dialami, M. Chiumenti, M. Cervera, R. Rossi, U. Chasco, and M. Domingo, Numerical and experimental analysis of the structural performance of AM components built by fused filament fabrication, Int. J. Mech. Mater. Des., vol. 17, no. 1, pp. 225-244, 2021. DOI: 10.1007/s10999-020-09524-8.
- I. Rivet, N. Dialami, M. Cervera, M. Chiumenti, G. Reyes, and M.A. Pérez, Experimental, computational, and dimensional analysis of the mechanical performance of fused filament fabrication parts, Polymers., vol. 13, no. 11, pp. 1766, 2021. DOI: 10. 3390/polym13111766.
- Q. Sun, G. Rizvi, C. Bellehumeur, and P. Gu, Effect of processing conditions on the bonding quality of FDM polymer filaments, Rapid Prototyp. J., vol. 14, no. 2, pp. 72-80, 2008. DOI: 10.1108/13552540810862028.
- Halil L. Tekinalp, Vlastimil Kunc, Gregorio M. Velez-Garcia, Chad E. Duty, Lonnie J. Love, Amit K. Naskar, Craig A. Blue, and Soydan Ozcan, Highly oriented carbon fiber-polymer composites via additive manufacturing, Compos. Sci. Technol., vol. 105, pp. 144-150, 2014. DOI: 10.1016/j.compscitech.2014.10.009.
- S. Garzon-Hernandez, D. Garcia-Gonzalez, A. J'Erusalem, and [42] A. Arias, Design of FDM 3D printed polymers: An experimental-modelling methodology for the prediction of mechanical properties, Mater. Des., vol. 188, pp. 108414, 2020. DOI: 10. 1016/j.matdes.2019.108414.
- B. Tymrak, M. Kreiger, and J.M. Pearce, Mechanical properties of components fabricated with open-source 3-D printers under realistic environmental conditions, Mater. Des., vol. 58, pp. 242-246, 2014. DOI: 10.1016/j.matdes.2014.02.038.
- L. Li, Q. Sun, C. Bellehumeur, and P. Gu, Composite modeling and analysis for fabrication of FDM prototypes with locally controlled properties, J. Manuf. Processes ., vol. 4, no. 2, pp. 129-141, 2002. DOI: 10.1016/S1526-6125(02)70139-4.
- Fillamentum Manufacturing Czech. PC/ABS datasheet, 2020. Available from https://fillamentum.com/wp-content/uploads/ 2020/10/Technical_Data_Sheet_PC-ABS.pdf.
- A. Forés-Garriga, M.A. Pérez, G. Gómez-Gras, and G. Reyes-Pozo, Role of infill parameters on the mechanical performance and weight reduction of PEI Ultem processed by FFF, Mater. Des., vol. 193, pp. 108810, 2020. DOI: 10.1016/j.matdes.2020.108810.
- P. Dadvand, R. Rossi, and E. Oñate, An object-oriented environment for developing finite element codes for multi-disciplinary applications, Arch. Comput. Methods Eng., vol. 17, no. 3, pp. 253-297, 2010. DOI: 10.1007/s11831-010-9045-2.
- Y. Rao, N. Wei, S. Yao, K. Wang, and Y. Peng, A process-structureperformance modeling for thermoplastic polymers via material extrusion additive manufacturing, Addit. Manuf., vol. 39, pp. 101857, 2021. DOI: 10.1016/j.addma.2021.101857.